Int. J. Heat Mass Transfer. Vol. 36, No. 15, pp. 3687–3695, 1993
Printed in Great Britain

0017–9310/93 $6.00 + 0.00

Upward solidification of a binary solution saturated porous medium

M. SONG, J. CHOI and R. VISKANTA
Heat Transfer Laboratory, School of Mechanical Engineering, Purdue University, West Lafayette, IN 47907, U.S.A.

(*Received* 12 *January* 1993 *and in final form* 31 *March* 1993)

Abstract—Upward solidification of a binary solution saturated porous medium was investigated experimentally and theoretically to identify the dominant physical phenomena and to document the experimental results. A solid matrix of the porous medium was a packed bed of glass beads, and the saturating liquid was an aqueous sodium chloride solution on the water-rich side of the eutectic composition. Freezing experiments were performed in a square cross-section enclosure under constant temperature conditions at the cold bottom and hot top walls. Transient temperature profiles and the liquidus and solidus positions were measured for different combinations of bead size, initial temperature and initial salt concentration. Simultaneous measurements of local concentration and temperature at selected locations were also made in a separate series of experiments. An analytical model, based on heat and species conservation principles and relations from the equilibrium phase diagram is suggested, and the predictions are compared with experimental data. The uniform distribution of the predicted average concentration suggests that species transport by diffusion is negligible, and the effect of bead size on the temperature profiles was confined to the region near the cold bottom. The behavior of dimensionless temperature under different initial temperature and concentration conditions could be explained by the relation between the local freezing rate and nonequilibrium undercooling. Also, the 'over-enriching' was observed in the mushy region away from the liquidus, but a quantitative analysis was not performed. The importance of incorporating models, which account for the effects of nonequilibrium undercooling and density differences between phases, and the need for experimental diagnostics, which do not disturb the physical phenomena occurring during the solidification of the mixture, are emphasized.

INTRODUCTION

SOLIDIFICATION of liquid saturated porous media occurs in a wide variety of applications in geophysics and engineering. Examples include seasonal freezing of soil, artificial freezing of ground as a construction technique for supporting poor soils, insulation of underground buildings, latent heat of fusion thermal energy storage in porous media and production and storage of frozen foods. Metallurgical applications include manufacturing of composite materials and purification of metals.

All phase change problems have in common a nonlinearity resulting from the moving solid/liquid interface, where absorption or liberation of latent energy occurs. For solidification of binary alloys under off-eutectic conditions, the process can be highly complicated, involving buoyancy-driven convection and morphological instabilities in the growth of the solid phase, which result in inhomogeneities and imperfections in the final product. Using shadowgraph, particle tracking and dye injection into the mushy region, a detailed photographic investigation on directional solidification of a binary mixture has revealed an array of complicated fluid motions [1], and reference is made to this study for the details. Extensive reviews concerning the transport phenomena during the solidification of binary mixtures are available [2, 3], and only the studies directly relevant to the present work will be reviewed.

Upward solidification of a binary alloy in the absence of solid matrix has been studied both theoretically [4–9] and experimentally [7, 9]. Huppert and Worster [7] developed a simple solidification model incorporating a mushy layer, in which solid and melt phases coexist. The good agreement between their experimental results and the model predictions was somewhat surprising in view of the fact that the solid fraction was assumed uniform in the mushy layer. Worster [8] extended the analysis by allowing the solid fraction to change in both space and time. Braga and Viskanta [9] constructed a macroscopic model based on the conservation principles to determine the rate of solidification and to compute the temperature distribution in the system during the solidification of an aqueous ammonium chloride solution. In their study, the knowledge of the temperature distribution together with the thermodynamic equilibrium and constant average concentration assumptions yielded the local solid fraction as well as the local liquid concentration in the mushy region. Comparison between predictions and experimental results revealed good agreement. In all of the existing one-dimensional solidification models, fluid motion is neglected. However, even with a stabilizing thermal buoyancy force field, intense fluid motion can be generated by solutal buoyancy forces

NOMENCLATURE

C	concentration of solute [wt%]
c_p	specific heat [J kg^{-1} K^{-1}]
D	diffusion coefficient of NaCl in water [m^2 s^{-1}]
d	average bead diameter [mm]
f	volume fraction to the total volume of medium
g	mass fraction to the total mass of medium
H	height of cavity [mm]
h	total enthalpy [J kg^{-1}]
k	thermal conductivity [W m^{-1} K^{-1}]
L	specific latent energy difference between eutectic solid and ice phases [J kg^{-1}]
M	specific latent energy difference between liquid and ice phases [J kg^{-1}]
T	temperature [°C]
t	time [s]
x	vertical coordinate measured from the bottom [mm].

Greek symbols

ε	volume fraction of liquid phase to that of void
θ	dimensionless temperature, $(T-T_c)/(T_h-T_c)$
ξ	dimensionless vertical coordinate, x/H
ϕ	volume fraction of eutectic solid phase to that of void
ρ	density of void [kg m^{-3}]
$\bar{\rho}$	average density of medium [kg m^{-3}].

Subscripts

b	glass bead
c	cold
e	eutectic solid phase
eq	equilibrium
eut	eutectic
i	initial or ice phase
l	liquid phase
v	void.

or by other phenomena such as volume change during phase transformation and surface tension gradients. A review of fluid motions during solidification of binary mixtures from below, above, and from the side is available [10] and need not be repeated here.

While solidification of binary alloys has received considerable research attention, little work has been done on the subject of mixture saturated porous medium solidification. The literature dealing with the freezing of a pure liquid saturated porous medium is abundant and an extensive review is available [11]. Cao and Poulikakos [12] experimentally investigated the solidification of an aqueous ammonium chloride solution saturated packed bed of glass beads from above. The effect of initial salt concentration and bottom surface heating were examined. Disagreement between measured and predicted interface locations were attributed to the neglect of fluid motions in the theoretical model. Okada and Murakami [13] and Okada *et al.* [14] studied the solidification of a porous medium saturated with an aqueous binary solution from a vertical side wall in a rectangular test cell. In the analysis, the buoyancy-driven convection resulting from both the temperature and concentration gradients was taken into account. The temperature and concentration fields in the test cell were measured, and good agreement with predicted results was asserted. However, discussion about the differences between measured and predicted results was not made.

The present paper reports on an experimental and theoretical investigation on the upward solidification of an aqueous sodium chloride solution saturated packed bed of glass beads. The main objective of the paper is to identify the dominant physical phenomena, to determine which analytical models are appropriate for the solidification of porous media by examining the effects of bead diameter, initial superheat and initial salt concentration on the temperature and concentration profiles, and to document the experimental results.

EXPERIMENTAL APPARATUS AND PROCEDURE

Solidification of an aqueous sodium chloride solution saturated packed bed of glass beads was made in a square cross-section test cell with inner dimensions of 149.2 mm in height and width and 73.0 mm in depth. Figure 1 shows a schematic of the experimental apparatus. The vertical front, back and side walls of the test cell were made of 25 mm thick acrylic plates, which were covered with 50 mm thick Styrofoam insulation except for the brief moment while visual access was made to locate the interfaces. The horizontal bottom and top walls were copper plates of the heat exchangers, having multiple coolant flow passages, and served as hot and cold walls. Fifteen liquid-tight holes were drilled along the center line of each vertical sidewall at equal intervals between $\xi = 0.07$ and 0.93 to allow for the insertion of thermocouples and hypodermic needles. The test assembly, including the insulation, was placed on the aluminum plate with leveling screws to eliminate any buoyancy-driven material convection current due to the inclination of the test cell.

The preparation of each experiment included constructing the solid matrix, saturating it with the desired solution and establishing uniform initial temperature and concentration conditions. Spherical soda-lime glass beads, having an average diameter of

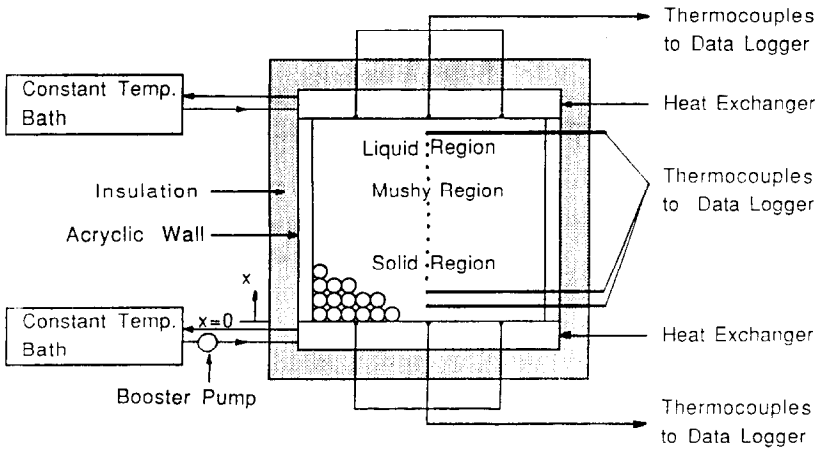

FIG. 1. Schematic diagram of the test apparatus.

either 2.85 or 6.0 mm, constituted the solid matrix and were first packed into the test cell. Thermocouples and sampling hypodermic needles were carefully inserted into the test cell one after another as the test cavity was filled with beads. The uncertainties in the vertical location of the probe tips were less than ± 1.0 mm. Next, deionized water with a resistivity larger than 15 Mohm-cm was mixed with the requisite amount of research grade sodium chloride grains to obtain the predetermined concentrations (± 0.02 wt%), and the solution was slowly siphoned into the test cell (about 0.9 $cm^3 s^{-1}$) to avoid entrainment of air bubbles.

Heat exchangers were connected to two constant temperature baths (NESLABULT-80DD and HAAKE A82) which used ethyl alcohol as the coolant. With appropriate valve settings between heat exchangers and constant temperature baths, the bottom and top walls of the test cell could be maintained either at the same temperature to achieve an initial uniform temperature condition or at different temperatures during the freezing experiment. The temperature of the hot top wall was maintained at the initial temperature throughout the run while the bottom surface temperature was rapidly dropped at the beginning of an experiment. In the preliminary test, it took more than 20 min for the bottom surface to reach the desired cold wall temperature from the initial value due to the small capacity of internal bath pumps. A booster pump was installed on the discharge side of the constant temperature bath to increase the coolant flow rate through the cold bottom heat exchanger. With the cold bath temperature several degrees lower than the predetermined cold wall temperature, the bottom surface temperature reached the desired temperature (-39.4°C) in less than 5 min. Thereafter, the cold bath temperature was slowly increased toward the predetermined cold wall temperature, and the cold bottom and hot top surface temperatures could be maintained within ± 0.2°C of the desired temperatures after about 1 h of freezing. Five thermocouples, placed in the copper plates close to the surface contacting the porous medium, insured the uniformity of the temperature along the top and bottom wall.

Temperature and concentration measurements were made separately to minimize heat gains from the ambient surroundings by reducing the number of probes. Fifteen type-T thermocouples were calibrated with an accuracy of ± 0.1°C and placed along the vertical center line of the test cell. Measured temperatures were recorded by an HP3497 data acquisition system with a time interval of 150 s. To determine the local concentration along the vertical center line, a few drops of solution were extracted through hypodermic needles and their refractive index were measured with a Kernco hand refractometer every 20 min.

During the solidification of a porous medium saturated with an off-eutectic concentration solution, three distinct regions exist (as is the case for the binary mixture solidification in the absence of solid matrix); the already solidified and fully unsolidified regions are separated by an extensive region where solidification is occurring. These three regions will be referred to as solid, liquid and mushy regions according to the phases occupying the void of the solid matrix. Also, the interfaces between liquid and mushy regions and between mushy and solid regions are referred to as liquidus and solidus. Liquidus and solidus were visually located and the relative positions from the bottom were measured every 20 min through the vertical front wall.

ANALYTICAL MODEL

The theoretical model for the solidification of a sodium chloride solution saturated porous medium is based on the conservation principles and the phase diagram. To aid in the discussion, the equilibrium phase diagram of the H_2O–NaCl mixture is given in Fig. 2. Pure ice is in equilibrium with the hypoeutectic concentration solution along the liquidus, while the composite of ice and eutectic composition solid is in

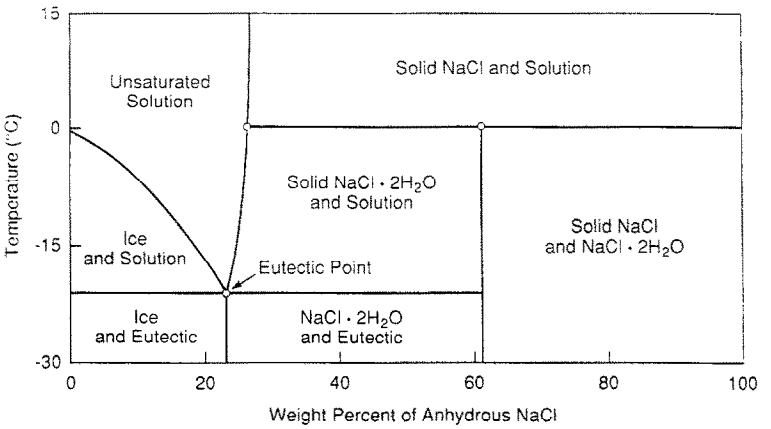

FIG. 2. Equilibrium phase diagram of aqueous sodium chloride solution.

equilibrium with eutectic composition solution (23.31 wt%) at eutectic temperature (−21.1°C). The space between the glass beads is occupied by the ice (subscript i) and liquid (subscript l) phases in the mushy region and by the ice and eutectic solid (subscript e) phases in the solid regions.

Since the temperature of maximum density is lower than the equilibrium liquidus temperature for the liquid concentration range of this study, both thermal and solutal buoyancy forces stabilize the flow. The analysis assumes that heat and mass transfer are one-dimensional and by diffusion only. To be consistent with the stagnant fluid assumption, the densities of liquid, ice and eutectic solid phases are assumed to be constant and same ($\rho_l = \rho_i = \rho_e$ = constant). Other thermophysical properties are assumed to be independent of temperature and concentration but different for each phase. Also, the thermal and phase equilibria are assumed. In the mushy region, the temperatures of ice and liquid phases are the same and their relations to the local liquid concentration are represented by the liquidus of the equilibrium phase diagram. The latent heat difference between liquid and ice phases is assumed to be independent of liquid concentration, and the difference between eutectic solid and ice phases is assumed different from zero considering the salt concentration of the eutectic solid phase (23.31 wt%). With the species diffusion through solid phases neglected, the model equations for heat and species transport are

Energy

$$\frac{\partial}{\partial t}(\bar{\rho}h) = \frac{\partial}{\partial x}\left(k\frac{\partial T}{\partial x}\right). \tag{1}$$

Species

$$\frac{\partial}{\partial t}(\bar{\rho}C) = \frac{\partial}{\partial x}\left(\rho\varepsilon D\frac{\partial C_l}{\partial x}\right). \tag{2}$$

In the above equations

$$h = c_p T + g_v(\phi M + \varepsilon L) \tag{3}$$

and

$$C = \phi C_{eut} + \varepsilon C_l \tag{4}$$

where ϕ and ε are mass (or volume) fractions of eutectic and liquid phases to the mass (or volume) of the void, while g represents the mass fraction to the total mass of the porous medium. Note the difference between volume averaged density of the porous medium ($\bar{\rho}$) and the density of the void (ρ)

$$\bar{\rho} = f_b\rho_b + f_v\rho \tag{5}$$

and

$$\rho = \rho_i = \rho_e = \rho_l. \tag{6}$$

The mass averaged specific heat and the volume averaged effective thermal conductivity are defined as

$$c_p = g_b c_{pb} + g_v[(1-\varepsilon-\phi)c_{pi} + \phi c_{pe} + \varepsilon c_{pl}] \tag{7}$$

$$k = f_b k_b + f_v[(1-\varepsilon-\phi)k_i + \phi k_e + \varepsilon k_l]. \tag{8}$$

Among the various models for the effective thermal conductivity, the volume averaged model is chosen for simplicity since the values predicted by the other models (for example, the Veinberg model [15]) differ less than 2%. The thermophysical properties used in the calculations are summarized in Table 1.

The initial and boundary conditions for the transport equations are

$$T = T_h, \quad C = C_i, \quad \phi = 0, \quad \varepsilon = 1 \quad \text{at} \quad 0 < x < H \quad \text{and} \quad t = 0 \tag{9}$$

$$T = T_c, \quad \frac{\partial C}{\partial x} = 0 \quad \text{at} \quad x = 0 \tag{10}$$

$$T = T_h, \quad \frac{\partial C}{\partial x} = 0 \quad \text{at} \quad x = H. \tag{11}$$

To solve for the six independent variables (h, T, C, C_l, ϕ, ε), two additional equations are required

Table 1. Thermophysical properties in the theoretical model

ρ_b [kg m^{-3}]	2370	ρ [kg m^{-3}]	1080
c_{pb} [J (kg K)$^{-1}$]	828	k_b [W (m K)$^{-1}$]	1.17
c_{pi} [J (kg K)$^{-1}$]	1950	k_i [W (m K)$^{-1}$]	2.03
c_{pe} [J (kg K)$^{-1}$]	1690	k_e [W (m K)$^{-1}$]	1.91
c_{pl} [J (kg K)$^{-1}$]	3690	k_l [W (m K)$^{-1}$]	0.555
L [J kg^{-1}]	3.38×10^5	M [J kg^{-1}]	6.23×10^4
H [mm]	149.2	D [m^2 s^{-1}]	1.61×10^{-9}

together with equations (1)–(4). The relations are obtained from the phase diagram

$$\varepsilon = 1, \quad \phi = 0 \quad \text{in the liquid region} \tag{12}$$

$$C_l = C_{eq}(T), \quad \phi = 0 \quad \text{in the mushy region} \tag{13}$$

$$C_l = C_{eut}, \quad T = T_{eut} \quad \text{at solidus} \tag{14}$$

$$C_l = C_{eut}, \quad \varepsilon = 0 \quad \text{in solid region.} \tag{15}$$

The transport equations (equations (1) and (2)) are discretized utilizing the control volume formulation and a fully implicit scheme. The harmonic-mean formulation is employed in evaluating heat and species diffusion coefficients. The main difficulties encountered were in dealing with the relations obtained from the phase diagram (equations (12)–(15)). The locations of liquidus and solidus are not known a priori, and an iterative procedure is necessary to advance each time step. In each iteration, the discretized conservation equations are solved for the total enthalpy (h) and average concentration (C), and then the fraction of the liquid phase (ε) and the fraction of the eutectic solid phase (ϕ) are determined. In the procedure to solve for ε and ϕ, a similar method developed by Prakash and Voller [16] was utilized with modifications to accommodate for the existence of the solid matrix and different thermophysical properties of the three phases. The time step was 0.5 s initially and was gradually increased by 1% of the previous time step to assure small changes in the liquid and eutectic solid fractions at each time step. A total number of 52 node points was employed for the numerical results reported in this paper, while the predicted solidus locations differed less than 0.5% from the predicted values using 102 nodes. Calculation times ranged between 50 and 60 CPU s on a CYBER 205 computer for a simulation time of 9 h.

RESULTS AND DISCUSSION

Experiments were conducted for two different glass bead sizes, two different initial temperatures and three different initial concentrations. The experimental conditions for the seven experiments discussed in this paper are summarized in Table 2. In all cases, three distinct regions (solid, mushy and liquid regions) came into existence. Experiments 1–5 were performed to measure the temperature distribution along the vertical center line of the cavity, and experiments 6 and 7 were performed to measure the simultaneous concentration and temperature variations at fewer selected locations during solidification. The scatter in the initial temperature is due to the difficulty in attaining the uniform temperature profile. In the preliminary test run, it took more than 30 h for the core temperature to drop to the desired range (initial temperature ± 0.2°C). Therefore, about 10 h after the top and bottom surfaces had been kept at a few degrees lower than the desired temperature, the hot bath temperature was readjusted close to the core temperature and maintained for several more hours before the solidification was started. The uniformity of the initial temperature profiles was better than ± 0.3°C.

Figure 3 shows the typical transient temperature readings measured along the vertical center line of the cavity at equal spacial intervals from $\xi = 0.07$ to 0.93 for experiment 2. The smooth trends and relatively even distribution of measured temperatures imply that the solidification rate is slow and advective heat transfer is absent. The same data are compared with the predicted temperatures in Fig. 4. The good agreement between measured and predicted temperatures suggest that the analytical model can be used to investigate the effects of various parameters controlling solidification. Note that measured temperatures are slightly higher near the cold bottom and a little lower near the liquidus in the mushy region than the predicted values.

Also shown in Fig. 4 are the results of the Neumann–Stefan type analysis well known in the literature [11]. Besides all the asumptions made in the present model of this study, the following additional assumptions are needed to obtain the closed form solutions: (1) species diffusion in the liquid phase is negligible and local average concentration remains the same as the initial concentration; (2) the liquid fraction (ε) is a linear function of local temperature in the mushy region; and (3) the freezing porous medium is semi-infinite. The results of the analytic model described in the previous section assured that the first assumption is reasonable under the experimental conditions of this study. However, the second and the third assumptions yielded temperatures which are significantly higher in the solid and mushy region and lower near the top wall. Also, the thickness of solid and mushy regions are seriously underpredicted by the Neumann–Stefan type model, as shown in Fig. 5, in spite of the semi-infinite domain assumption.

In Fig. 5, the visually observed solidus and liquidus locations are compared with the predictions of the

Table 2. Summary of experimental conditions

Exp.	C_i (%)	T_{eq} (°C)	d (mm)	T_c (°C)	$T_h = T_i$ (°C)	f_s
1	5	−3.0	2.85	−39.4	9.7	0.397
2	5	−3.0	6.0	−39.4	9.6	0.396
3	5	−3.0	6.0	−39.4	4.0	0.396
4	10	−6.5	6.0	−39.4	4.0	0.396
5	15	−10.7	6.0	−39.4	9.9	0.396
6	10	−6.5	6.0	−39.4	3.8	0.396
7	15	−10.7	6.0	−39.4	3.5	0.396

Experiments 1–5 were conducted to measure the temperature distributions. Experiments 6 and 7 were for simultaneous measurements of temperature and concentration.

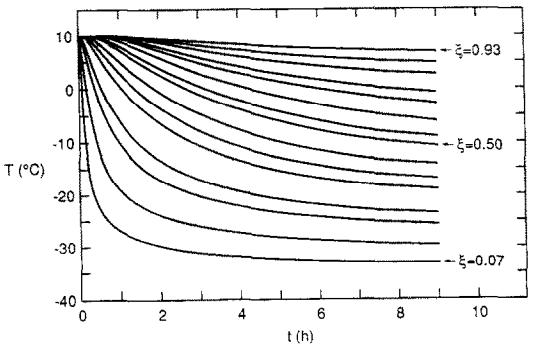

FIG. 3. Typical transient temperature readings (experiment 2).

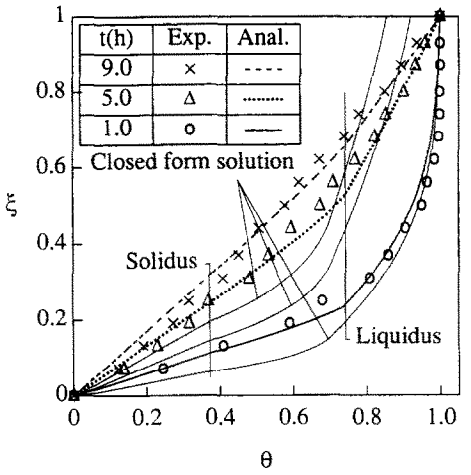

FIG. 4. Temperature distributions at the vertical center line of the test cell (experiment 2).

analytic models and with the locations determined from the measured temperature data (Fig. 4). The differences between the two sets of experimental data can be explained as follows. The first reason is due to the equilibrium assumptions embedded in evaluating the solidus and liquidus locations from the temperature profiles. Owing to the formation of a solute-rich liquid layer on a microscopic scale adjacent to the ice phase during solidification, the microscopic distribution of the liquid concentration in the mushy region becomes highly nonuniform when the time for the solute transport is not sufficient [17]. The local

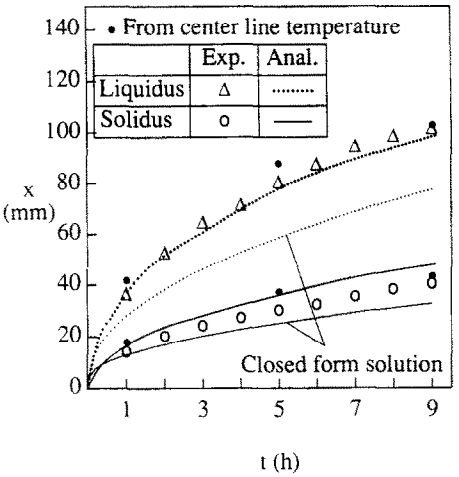

FIG. 5. Liquidus and solidus locations (experiment 2).

temperature, corresponding to the higher liquid concentration at the interface between the ice and liquid phases, is lower than the equilibrium liquidus temperature corresponding to the macroscopic liquid concentration (nonequilibrium undercooling [2, 3]). The real liquidus and solidus locations may match the lower local temperatures rather than the equilibrium solidus and liquidus temperatures. The second reason is due to the different measuring locations. In the vicinity of the front wall, where the visual access is confined to, the advance of the solidus and liquidus are delayed due to the heat gain from the ambient surroundings. The validity of the first contribution will be further assessed in the later discussion.

Transient variations in the measured and predicted dimensionless temperature under the same experimental conditions (except for the different bead sizes) are compared in Fig. 6. The effect of the bead size mainly originates from the existence of the thin region adjacent to the walls, where the void fraction increases rapidly towards the wall reaching unity at the wall. The predicted temperatures for different bead sizes are almost the same, because the effect is reflected only by the small difference in the average void fractions (0.377 and 0.396). As the void fractions were determined by measuring the increase in the level after the known volume of water was slowly introduced, the difference in the local void fraction near the vertical

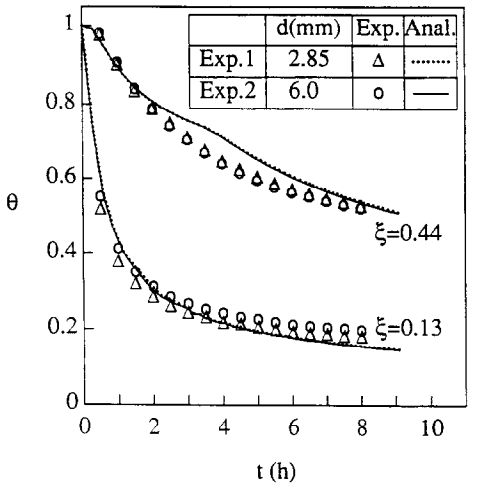

FIG. 6. Effect of bead diameter on dimensionless temperature.

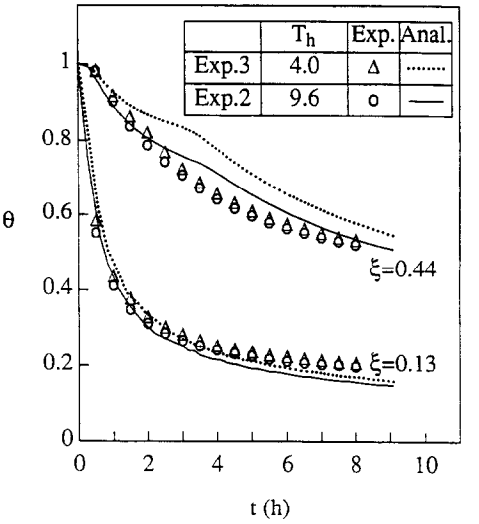

FIG. 7. Effect of liquid superheat on dimensionless temperature.

side walls was reflected in the small difference of the average void fractions. The effect of the bead size on the measured temperature was most significant at $\xi = 0.13$. With the larger diameter beads, the measured dimensionless temperature near the cold bottom is higher due to the increase in the thickness of the high void fraction layer adjacent to the bottom wall. The latent energy to be removed during the solidification and the heat capacity of the medium are larger in this layer owing to the high void fraction and the larger heat capacity of the phase changing material than that of the glass bead. The slightly higher measured temperatures compared to the predicted values near the cold bottom in Fig. 4 are now explained by the effect of the thin high void fraction layer adjacent to the bottom wall. Near the hot top surface, the medium does not undergo either the solidification or the drastic change in temperature, and the effect of the bead size on the dimensionless temperature is not significant. When the system is solidified from the top cold wall, the same explanation is valid [18].

Figure 7 illustrates the effect of the initial superheat and the top wall temperature. The difference in the dimensionless temperature under the different initial temperature is well predicted at $\xi = 0.13$, which corresponds to the solid region for practically the entire duration of the experiment. Again, the slightly higher measured temperature is due to the high void fraction layer adjacent to the cold bottom as discussed above. The dimensionless temperature at $\xi = 0.44$ is overpredicted by a larger fraction when the initial superheat is smaller, which corresponds to the mushy region for the entire duration of the experiment. When the initial (and hot top wall) temperature is lower, the solidification rate is larger and the nonequilibrium undercooling is greater. Since the present analytical model assumes phase equilibrium, the change in the dimensionless temperature under the different initial temperatures is overpredicted.

The same explanation is appropriate for the effect of the initial concentration. As the initial concentration is closer to the eutectic composition, the equilibrium liquidus temperature is lower, and the solidification rate is smaller. Hence, the dimensionless temperature at $\xi = 0.44$ is overpredicted by the smaller fraction (Fig. 8). For the case of the smallest solidification rate with the highest initial temperature and concentration (experiment 5), the agreement between predicted and measured temperatures is the best (Fig. 9). The nonequilibrium undercooling weakens the impact of different initial concentrations on the dimensionless temperature in the mushy region. Suffice it to say that the lower measured temperatures compared to the predicted values in the mushy region are due to the nonequilibrium undercooling.

To further investigate the nonequilibrium under-

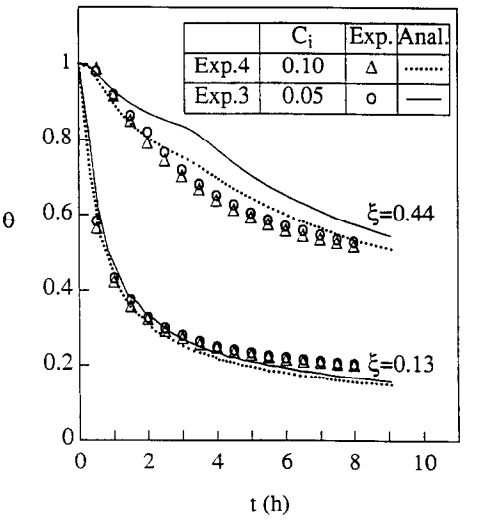

FIG. 8. Effect of initial concentration on dimensionless temperature under a relatively lower initial temperature condition.

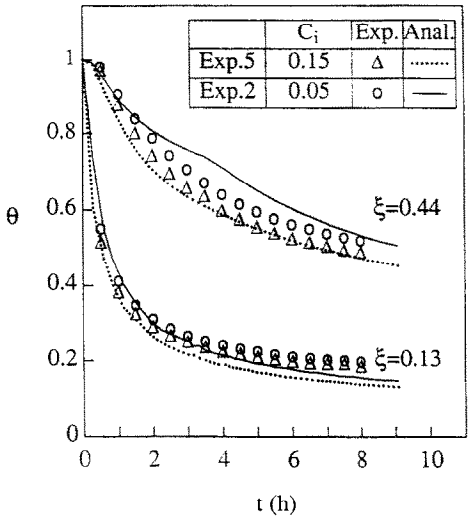

FIG. 9. Effect of initial concentration on dimensionless temperature under a relatively higher initial temperature condition.

cooling, the behavior of the local liquid concentration is examined in experiments 6 and 7. In both experiments, a few drops of saline solution were extracted through hypodermic needles whose tips were located on the vertical center line at $\xi = 0.25$, 0.31 and 0.80. There was no concentration variation during the freezing process at $\xi = 0.80$, and the comparisons between the measured and predicted liquid concentrations at $\xi = 0.25$ are shown in Fig. 10. The predicted liquid concentration starts to increase drastically as the liquidus passes, and the rate of change levels off as the eutectic composition is approached. The measured liquid concentration displays gradual changes near the liquidus and approaches the predicted values at later times. Near the solidus the local solidification rate is retarded, and the characteristic length for the diffusion of the rejected solute decreases as the liquid fraction decreases; therefore, non-

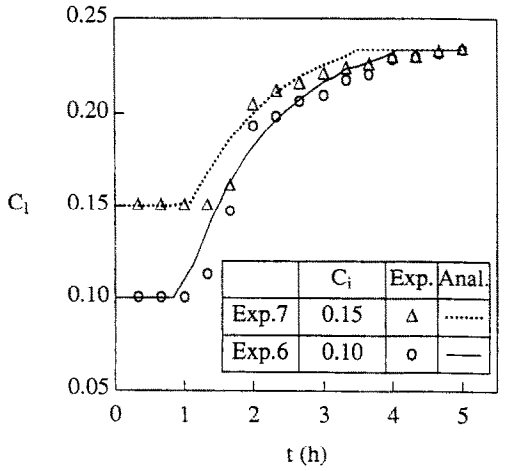

FIG. 10. Transient liquid concentration at $\xi = 0.25$.

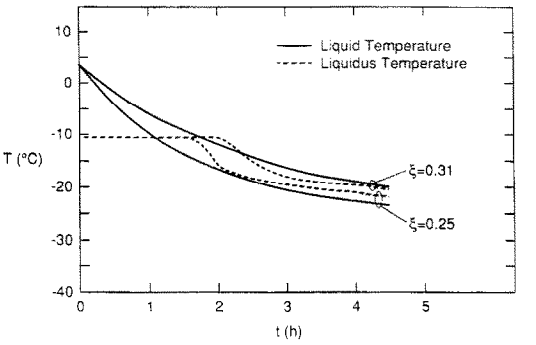

FIG. 11. Result of simultaneous temperature and liquid concentration measurement (experiment 7).

equilibrium undercooling cannot be maintained. In Fig. 11, the equilibrium liquidus temperature evaluated from the measured liquid concentration is shown together with the simultaneously measured temperature for the slowest freezing case (experiment 7). Close to the cold bottom wall ($\xi = 0.25$), the medium temperature was lower than the equilibrium liquidus temperature throughout the freezing process since the nonequilibrium undercooling, maintained by the high freezing rate, was dominant. However, a little further from the cold wall ($\xi = 0.31$), the equilibrium liquidus temperature was lower than the medium temperature, except for the short period following after the liquidus passing. The maximum amount of this 'over-enriching' was 2.1 wt% (equivalent to 1.9°C) for the initial concentration of 15% and was 3.1 wt% (equivalent to 2.8°C) for the initial concentration of 5%, at $\xi = 0.31$. A possible explanation for the over-enriching is thought to be the effect of the solute-enriched liquid flowing through the mushy region driven by the expansion or contraction during the phase transformation. The density of the liquid phase is larger than that of the ice phase and smaller than that of the eutectic solid phase for the H_2O–NaCl mixture. Even though the uncertainty involved in measuring the concentration of extracted liquid is less than $+0.2$ wt%, the present concentration measuring technique is not sufficiently accurate for a quantitative study of 'over-enriching' phenomena, since the frequent extraction of sample solution may override the effect of the flow due to volume change by producing a point volume sink. Further studies should be carried out with an analytical model which accounts for the effects of nonequilibrium undercooling and for the density difference between the phases together with the concentration measuring technique which does not disturb the physical phenomena occurring during solidification of the mixture.

CONCLUSIONS

Upward solidification of an aqueous sodium chloride solution saturated packed bed of glass beads in a square cross-section enclosure was investigated experimentally and theoretically. A number of freezing

experiments were performed for different combinations of bead diameter, initial temperature and initial concentration to measure the transient temperature profiles and the liquidus and solidus locations. Simultaneous local concentration and temperature measurements at selected locations were also made in a separate series of experiments. The analytical models based on the heat and species conservation principles and the equilibrium phase diagram were proposed, and the results revealed that species diffusion can be neglected under the experimental conditions of this study.

In general, the measured temperatures agreed well with the predicted values, but the measured temperatures were slightly higher near the cold bottom surface and a little lower in the mushy region, especially near the liquidus. With the larger diameter beads, the measured dimensionless temperature near the cold bottom is higher than the predicted values by a larger fraction, due to the increase in the thickness of the high void fraction layer adjacent to the bottom wall. This is owing to the fact that the latent energy to be removed during the solidification and the heat capacity of the medium are larger in this layer. The effect of bead size on the temperature profile away from the cold bottom wall was not significant.

Nonequilibrium undercooling existed in the mushy region and weakened the impact of change in initial temperature and/or initial concentration on the dimensionless temperature, because the amount of undercooling increased as the local freezing rate increased. The examination of the simultaneously measured concentration and temperature revealed that 'over-enriching' may occur in the mushy region away from the liquidus, as the effect of advective flow, induced by the volume change during the phase transformation, counterbalances the effect of the nonequilibrium undercooling. Further quantitative analysis was not carried out due to the interfering nature of the concentration measuring technique employed. There is a need for analytical models, which accommodate the effect of nonequilibrium undercooling and the effect of density differences between phases. Experimental diagnostics for the measurement of liquid concentration, which do not disturb the physical phenomena occurring during the solidification of the mixture, are also needed.

REFERENCES

1. C. S. Magirl and F. P. Incropera, Flow and morphological conditions associated with undirectional solidification of aqueous ammonium chloride. In *Topics in Heat Transfer*, HTD-Vol. 206-1, pp. 1–9. ASME, New York (1992).
2. R. Viskanta, Mathematical modeling of transport processes during solidification of binary systems, *JSME Int. J., Ser. 2* **33,** 409–423 (1990).
3. R. Viskanta, Transport phenomena during solidification of binary systems. In *Proceedings of the 4th Brazilian Thermal Science Meeting, Rio de Janeiro* (Edited by L. F. A. Azevedo, S. L. Braga and C. V. M. Braga), pp. P-39–P-50. Brazilian Society of Mechanical Engineers, Rio de Janeiro (1992).
4. S. H. Cho and J. E. Sunderland, Heat conduction problems with melting or freezing, *J. Heat Transfer* **91,** 421–426 (1969).
5. M. G. O'Callaghan, E. G. Cravalho and C. E. Huggins, Instability of the planar freeze front during solidification of an aqueous binary solution, *J. Heat Transfer* **102,** 673–677 (1980).
6. Y. Hayashi and T. Komori, Investigation of freezing of salt solution in cells, *J. Heat Transfer* **101,** 459–464 (1979).
7. H. E. Huppert and M. G. Worster, Dynamic solidification of a binary melt, *Nature* **314,** 703–707 (1985).
8. M. G. Worster, Solidification of an alloy from a cooled boundary, *J. Fluid Mech.* **167,** 481–501 (1986).
9. S. L. Braga and R. Viskanta, Solidification of a binary solution on a cold isothermal surface, *Int. J. Heat Mass Transfer* **33,** 745–753 (1990).
10. H. E. Huppert, The fluid mechanics of solidification, *J. Fluid Mech.* **212,** 209–240 (1990).
11. R. Viskanta, Phase change heat transfer in porous media. In *Proceedings of the Third International Symposium on Cold Regions Heat Transfer* (Edited by Z. P. Zarling), pp. 1–24. University of Alaska, Fairbanks (1991).
12. W. Z. Cao and D. Poulikakos, Freezing of a binary alloy saturating a packed bed of spheres, *J. Thermophys. Heat Transfer* **5,** 46–53 (1991).
13. M. Okada and M. Murakami, Solidification of porous media saturated with aqueous solution in a rectangular cell. In *Proceedings of the 27th National Heat Transfer Symposium of Japan*, Vol. 1, pp. 241–243. Heat Transfer Society of Japan, Tokyo (1990).
14. M. Okada, K. Matsumoto, M. Murakami and Y. Yabushita, Solidification of porous media saturated with aqueous solution in a rectangular cell. In *Proceedings of the 28th National Heat Transfer Symposium of Japan*, Vol. 1, pp. 304–306. Heat Transfer Society of Japan, Tokyo (1991).
15. A. K. Veinberg, Permeability, electrical conductivity, dielectric constant and thermal conductivity of a medium with spherical and ellipsoidal inclusions, *Sov. Phys. Dokl.* **11,** 593–595 (1967).
16. C. Prakash and V. Voller, On the numerical solution of continuum mixture model equations describing binary solid–liquid phase change, *Numer. Heat Transfer* **15,** 171–189 (1989).
17. A. Ohno, *The Solidification of Metals*, Chap. 8. Chijin Shokan, Tokyo (1976).
18. J. Choi and R. Viskanta, Freezing of aqueous sodium chloride solution saturated packed bed from above. In *Topics in Heat Transfer* (Edited by E. Toner), HTD-Vol. 206-2, pp. 159–166. ASME, New York (1992).